HAL
open science

Antiferromagnetic order and the structural order-disorder transition in the Cd6Ho quasicrystal approximant

A. Kreyssig, Guillaume Beutier, T. Hiroto, M.G. Kim, Gregory S. Tucker, Marc de Boissieu, R. Tamura, A.I. Goldman

To cite this version:

A. Kreyssig, Guillaume Beutier, T. Hiroto, M.G. Kim, Gregory S. Tucker, et al.. Antiferromagnetic order and the structural order-disorder transition in the Cd6Ho quasicrystal approximant. Philosophical Magazine Letters, 2013, 93 (9), pp.512-520. 10.1080/09500839.2013.815375 . hal-00881261

HAL Id: hal-00881261

https://hal.science/hal-00881261

Submitted on 8 Nov 2013

HAL is a multi-disciplinary open access archive for the deposit and dissemination of scientific research documents, whether they are published or not. The documents may come from teaching and research institutions in France or abroad, or from public or private research centers.

L'archive ouverte pluridisciplinaire **HAL**, est destinée au dépôt et à la diffusion de documents scientifiques de niveau recherche, publiés ou non, émanant des établissements d'enseignement et de recherche français ou étrangers, des laboratoires publics ou privés.

Antiferromagnetic order and the structural order-disorder transition in the Cd_6Ho quasicrystal approximant

Andreas Kreyssig[1], Guillaume Beutier[2], Takanobu Hiroto[3], Min Gyu Kim[1], Gregory Tucker[1], Marc de Boissieu[2], Ryuji Tamura[3] and Alan I. Goldman[1]

[1]*Ames Laboratory, U. S. DOE and Department of Physics and Astronomy, Iowa State University, Ames, Iowa 50011, USA*

[2]*SiMAP, Grenoble – UMR 5266 CNRS Grenoble-INP UJF, BP 75, 38402 Saint Martin d'Hères, France*

[3]*Department of Materials Science and Technology, Tokyo University of Science, Noda, JP-278-8510, Japan*

Antiferromagnetic order and the structural order-disorder transition in the Cd_6Ho quasicrystal approximant

We have used x-ray resonant magnetic scattering at the Ho L_3-edge to elucidate the nature of the antiferromagnetic ordering below T_N = 8.5 K in Cd_6Ho. The magnetic Bragg peaks are found at the charge forbidden $H + K + L = 2n+1$ positions, referenced to the high-temperature body-centered cubic structure. In general terms, this corresponds to antiferromagnetic arrangements of the Ho moments on adjacent clusters in the unit cell. In contrast to previous studies of Cd_6Ho, we find that there is an abrupt (first-order) transition to a monoclinic structure below $T_S \approx$ 178 K and conclude that this may be a general feature of those Cd_6R (R = rare earth) compounds that order magnetically.

Keywords: quasicrystal; approximant; antiferromagnetism

1. Introduction

Since publication of the discovery of icosahedral quasicrystals by Dan Shechtman in 1984 [1], the nature of the electronic properties of aperiodic systems and, in particular, the intriguing possibility of long-range antiferromagnetic order in quasicrystals, has stimulated a large volume of experimental and theoretical work. To date, however, no "quasi-antiferromagnets" have been discovered and, until very recently, even those periodic approximants to icosahedral quasicrystals that feature local moments (e.g. rare-earth ions), exhibit spin-glass-like behaviour at best [2,3]. The recent evidence for long-range antiferromagnetic order in the Cd_6R (R = rare earth) 1/1 approximants to the Cd-Mg-R quasicrystals offered by magnetic susceptibility and specific heat measurements [4-6], confirmed by scattering experiments [7], has reinvigorated investigations of magnetism in quasicrystals and related periodic approximants. Indeed, the Cd_6R 1/1 approximants present fascinating structural and magnetic behaviour in addition to the simplicity of binary alloys relative to ternary and higher alloys.

The room-temperature structure of the Cd_6R 1/1 approximants may be described as a body-centered cubic (bcc) packing of interpenetrating Tsai-type icosahedral clusters [8,9], which are composed of four successive shells with a Cd tetrahedron at the center. The first shell is a dodecahedron made of 20 Cd atoms, the second shell is an icosahedron of 12 *R* atoms, the third shell is an icosidodecahedron of 32 Cd atoms and the fourth shell is a rhombic triacontahedron of 60 Cd atoms. For the 1/1 Cd_6R approximants, the icosahedral clusters placed at the bcc lattice points interpenetrate neighboring clusters along the [111] directions.

For the lighter rare earths (*R* = Pr, Nd, Sm, Gd, Tb, Dy), a structural order-disorder transition has been reported at 150 K < T_S < 200 K such that, below T_S, the central Cd tetrahedra order along the [101] directions with alternating orientations [10-13]. This results in a doubling and distortion of the unit cell from the high-temperature cubic phase (*I m -3*) to a low-temperature monoclinic phase (*C 2/c*). However, for the heavier rare earths (*R* = Ho, Er, Tm, Lu), no structural transition has been observed [6, 14]. The difference in behaviour between the light and heavy rare earths was explained in terms of steric constraints imposed by the surrounding cages of Cd and *R* atoms. The decrease in the lattice constant that follows the lanthanide contraction correspondingly reduces the size of the cavity within the first dodecagonal Cd shell [9] and kinetically limits the reorientation of the Cd tetrahedra within this cage. This interpretation also seemed consistent with the results of pressure studies on Cd_6Yb [15].

For many of the Cd_6R alloys, anomalies in the magnetic susceptibility and specific heat measurements have been found that are consistent with long-range magnetic order. For example, relatively sharp transitions appear in the susceptibility and specific heat measurements, for Cd_6Tb, at approximately 24 K and 19 K [5,6]. The 24 K feature has been unambiguously identified as the transition from a paramagnetic

state to an antiferromagnetically ordered state by x-ray resonant magnetic scattering (XRMS) measurements [7]. The second feature at 19 K has not yet been identified with a significant change in the magnetic structure and is presently under investigation.

The connection, if any, between the antiferromagnetic order in the Cd_6R series and the higher-temperature structural distortion has not yet been established, although it was speculated that the monoclinic distortion might serve to relieve some degree of magnetic frustration inherent to the nearly perfect icosahedral arrangement of local moments found in the cubic structure [7]. Furthermore, the absence of a structural transition for Cd_6R alloys containing Ho, Er, Tm and Lu has been associated with a bifurcation of the de Gennes scaling of the Néel temperatures as well as differences in the electronic structure that result in a large residual resistivity at low temperature [6].

The present XRMS and high-energy x-ray diffraction studies of Cd_6Ho were undertaken to shed further light on this issue. Cd_6Ho was reported to retain its cubic symmetry to low temperature *and* order magnetically at T_N = 8.5 K [6]. Our scattering results show that the antiferromagnetic order for Cd_6Ho manifests the same general features as found for Cd_6Tb *and* there is clear evidence of the same structural order-disorder transition at T_S = 178 K. This transition is quite sharp in temperature and exhibits hysteresis, indicating a first-order character.

2. Experimental Details

Single crystals of Cd_6Ho were prepared by a self-flux method by melting high purity elements of Cd (99.9999 wt%) and Ho (99.9 wt%) in a 9:1 atomic ratio at 993 K for 24 hours in an alumina crucible sealed inside a quartz tube. This was followed by slow cooling at a rate of 2 K/hour to 773 K. The remaining Cd melt was then removed by means of a centrifuge, and the alloys were subsequently annealed at 923 K for 100

hours to improve the sample homogeneity, followed by further annealing at 473 K for 3 weeks to reduce point defects. Temperature dependent resistance measurements, as well as electron diffraction patterns taken at high and low temperature, showed no evidence of a structural order-disorder transition down to 20 K.

Since the naturally occurring isotope mixture of Cd is highly neutron absorbing, magnetic neutron-diffraction measurements are difficult without the appropriate isotopic substitution. Therefore, we have used XRMS to determine the nature of the magnetic order using a millimeter-sized single crystal with well-defined facets normal to the [1, 0, 0] direction. The XRMS measurement was performed on the 6-ID-B station at the Advanced Photon Source at the Ho L_3 absorption edge (E = 8.071 keV). The incident radiation was linearly polarized perpendicular to the vertical scattering plane (σ-polarized) with a beam size of 0.5 mm (horizontal) by 0.2 mm (vertical). In this configuration, dipole resonant magnetic scattering rotates the plane of linear polarization into the scattering plane (π -polarization). Pyrolytic graphite [PG (0, 0, 6)] was used as a polarization analyzer to suppress the charge and fluorescence background relative to the magnetic scattering signal.

In addition to the XRMS measurements, high-energy x-ray (E = 100.2 keV) diffraction patterns were recorded in station 6-ID-D at the APS. The use of high-energies minimizes sample absorption, so that the bulk of the sample is probed and large portions of the reciprocal lattice planes are recorded as the sample is rocked through two independent angles about axes perpendicular to the incident beam (see Ref. 16). The direct beam was blocked by a beam stop and diffraction images were recorded by a MAR345 image plate positioned 2862 mm behind the sample. The beam size was reduced to 0.5 mm by 0.5 mm using a slit system.

3. Results

The sample was mounted at the end of the cold finger of a closed-cycle refrigerator with the cubic (H, K, 0) plane coincident with the vertical scattering plane. For the balance of this paper, we will use the cubic notation of the high-temperature phase for the description of the reciprocal space and directions. Above 180 K, only a single Bragg diffraction peak was observed at the charge scattering allowed positions, $H + K + L = 2n$, (H, K, L, and n integer) of the bcc lattice. As the temperature was lowered an abrupt transition occurred resulting in a distribution of peaks about these positions, as illustrated in Figure 1 for the (10, 0, 0) reciprocal lattice point. Scans along the [H, 0, 0], [0, K, 0], and [0, 0, L] directions [Figs. 1(a), 1(b) and (c)] revealed at least five distinct domains as shown schematically in Figure 1(f). This distribution of scattering is very similar to what was previously observed for the monoclinic domains at low temperature for Cd_6Tb [7], although six rather than five domains were clearly observed in that case. The data in Figure 1, therefore, indicate the presence of a structural order-disorder transition in Cd_6Ho, at T_S = 178 K, that was previously undetected, potentially because the magnitude of the Bragg peak splitting found for Cd_6Ho is only roughly half of that for Cd_6Ho with weaker separation of peaks in the diffraction pattern.

The structural order-disorder transition in other Cd_6R alloys is also characterized by the appearance of superlattice peaks, below T_S, in electron diffraction patterns specified by the propagation vector (0, ½, ½) [10-13]. In Figure 2 we show a split-panel display of the high-energy x-ray diffraction patterns taken with the beam parallel to the [0, 0, 1], [1, 1, 0], and [1, 1, 1] directions of the sample both below (left side) and above (right side) T_S. The abovementioned superlattice reflections are clearly evidenced in Figures 2(b) and (c), below T_S, confirming the existence of the structural order-disorder

transition. These superlattice peaks were also observed during the XRMS measurement and the temperature dependence of the intensity of the (10, ½, ½) superlattice reflection is shown in Figure 3. Here, we see that the structural order-disorder transition is quite sharp in temperature and manifests a hysteresis of approximately 1-2 K on heating and cooling. Therefore, we conclude that this transition is most likely first-order in nature.

Below T_N = 8.5 K, additional magnetic Bragg scattering appeared close to points in reciprocal space corresponding to odd values of the sum $H + K + L = 2n + 1$ (H, K, L, and n integer) as illustrated in Figs. 1(d) and (e). These figures also show that magnetic Bragg peaks arise from all domains associated with the chemical structure and, as was also found for Cd_6Tb, the magnetic Bragg peaks are as sharp as the charge Bragg peaks, confirming the long-range character of the magnetic order in Cd_6Ho below T_N. The magnetic transition temperature (T_N = 8.5 K) derived from the magnetic susceptibility and specific heat measurements on this sample is in excellent agreement with the onset of magnetic order observed in the XRMS study as shown in Fig. 4. We also see here that all of the monoclinic domains manifest the same evolution of magnetic order as the temperature is lowered below T_N.

4. Discussion and Conclusions

Inasmuch as the Cd_6Ho sample studied here clearly manifests a structural order-disorder distortion at a temperature of T_S = 178 K that is comparable to that in other Cd_6R alloys, we are left with the question of why this was not observed in previous investigations. First, we note that the identification of the structural distortion is generally made by the observation of a kink in the temperature dependence of the resistivity at T_S, as found for the Cd_6R alloys with R = Pr, Nd, Sm Gd and Tb [6], but this feature is much less distinct in Cd_6Y and Cd_6Dy and related systems like Zn_6Sc [17, 18], so we must look beyond

these data. We further note that previous selected area electron diffraction patterns from Cd_6Ho showed no evidence of the superlattice peaks characteristic of the structural order-disorder transition at low temperatures [14]. However, it has also been established that the physical properties of the Cd_6R and Zn_6Sc quasicrystal approximants can be quite sensitive to alloy composition, sample preparation protocol and subsequent heat treatments [18]. One possible explanation for the difference observed here is that the sample used in the present study was stored at ambient temperature in an inert atmosphere for approximately one year after synthesis, and this resulted in subtle changes in the structural/chemical order of the sample. In support of this claim, Figure 3(b) displays a measurement of the temperature dependent resistance of the same sample measured in the XRMS experiment which now clearly shows a kink at T_S. We note, however, that the Néel temperature for the sample studied in the present investigation (T_N = 8.5 K) is the same as that found in previous investigations by other groups, arguing against significant differences in the magnetic properties.

Prior to this investigation, the absence of a structural order-disorder transition in the Cd_6R cubic approximants with R = Ho, Er, Tm, and Lu was generally accepted. As described in the Introduction, it was proposed that the decrease in the lattice constant due to the lanthanide contraction reduces the size of the cavity within the first dodecagonal Cd shell below a critical value (at R = Ho) and kinetically limits the reorientation of the Cd tetrahedral within this cage. Since we have clearly demonstrated that the structural distortion is present in Cd_6Ho, this proposal should be revisited and further structural investigations of the remaining Cd_6R with R = Er, Tm, and Lu seems necessary.

We have also found that the general features of the antiferromagnetic order in Cd_6Ho are the same as those found previously for Cd_6Tb [7]. With reference to the high

temperature bcc unit cell description of Cd_6Ho, the antiferromagnetic order breaks the body-centering translational symmetry of the chemical unit cell such that the Ho ions associated with the icosahedral cluster at the corner of the unit cell are antiferromagnetically correlated with the Ho ions associated with the icosahedral cluster at the center of the unit cell. The specific details of the magnetic structure (e.g. moment directions and configurations within a single icosahedral cluster) may, of course, differ between Cd_6Ho and Cd_6Tb (e.g. due to differences in the magnitude of the single-ion anisotropy). A complete specification of magnetic structure will first require a complete description of the chemical structure in the low-temperature monoclinic phase as well as the details of the chemical domain structure in this phase. Further analysis of the magnetic structure can then clarify whether the Ho moments are collinearly aligned or arranged in a more complex manner.

References

1. D. Shechtman, I. Blech, D. Gratias, and J.W. Cahn, Phys. Rev. Lett. **53**, 1951 (1984).
2. P. Wang, Z. M. Stadnik, K. al Qadi, and J. Przewo´znik, J. Phys.:Condens. Matter **21**, 436007 (2009).
3. S. Ibuka, K. Iida, and T. J. Sato, J. Phys.: Condens. Matter **23**, 056001 (2011).
4. R. Tamura, Y. Muro, T. Hiroto, K. Nishimoto, and T. Takabatake, Phys. Rev. B **82**, 220201(R) (2010).
5. R. Tamura, Y. Muro, T. Hiroto, H. Yaguchi, G. Beutier, and T. Takabatake, Phys. Rev. B **85**, 014203 (2012).
6. A. Mori, H. Ota, S. Yoshiuchi, K. Iwakawa, Y. Taga, Y. Hirose, T. Takeuchi, E. Yamamoto, Y. Haga, F. Honda *et al.* , J. Phys. Soc. Jpn. **81**, 024720 (2012).
7. M. G. Kim, G. Beutier, A. Kreyssig, T. Hiroto, T. Yamada, J. W. Kim, M. De Boissieu, R. Tamura and A. I. Goldman, Phys. Rev. B **85**, 134442 (2012).
8. C. P. Gomez and S. Lidin, Phys. Rev. B **68**, 024203 (2003).
9. S.Y. Piao, C.P. Gómez and S. Lidin, Z. Naturforsch. B **60** 644 (2006).
10. R. Tamura, K. Edagawa, K. Shibata, K. Nishimoto, S. Takeuchi, K. Saitoh, M. Isobe and Y. Ueda, Phys. Rev. B 72, 174211 (2005).
11. R. Tamura, K. Edagawa, C. Aoki, S. Takeuchi and K. Suzuki, Phys. Rev. B **68**, 174105 (2003).
12. R. Tamura, K. Edagawa, C. Aoki, S. Takeuchi and K. Suzuki, J. Alloys Compd. **378**, 290 (2004).
13. K. Nishimoto, R. Tamura and S. Takeuchi, Phys. Rev. B **81**, 184201 (2010).
14. K. Nishimoto, T. Sato, M. Muraki and R. Tamura, Phil. Mag. **91**, 2587 (2011).
15. T. Watanuki, A. Machida, T. Ikeda, K. Aoki, H. Kaneko, T. Shobu, T. J. Sato and A. P. Tsai, Phys. Rev. Lett. 96, 105702 (2006).
16. A. Kreyssig, S. Chang, Y. Janssen, J.-W. Kim, S. Nandi, J. Q. Yan, L. Tan, R. J. McQueeney, P. C. Canfield, and A. I. Goldman, Phys. Rev. B **76**, 054421 (2007).
17. J. Hasegawa, R. Tamura and S. Takeuchi, Phys. Rev. B **66**, 132201 (2002).
18. T. Ishimasa, Y. Kasano, A. Tachibana, S. Kashimoto and K. Osaka, Phil. Mag. **87**, 2887 (2007).
19. R. Tamura, Isr. J. Chem. **51**, 1263 (2011).

Figure Captions

Figure 1. Scans through the charge peaks at the bcc (10, 0, 0) diffraction peak position along the (a) [*H*, 0, 0], (b) [0, *K*, 0], and (c) [0, 0, *L*] directions illustrating the distribution of monoclinic domains below T_S. Panels (d) and (e) display the magnetic Bragg peaks, measured at $T = 1.6$ K, near the (7, 0, 0) charge-forbidden position. The positions of all measured charge peaks are shown schematically in panel (f).

Figure 2. High-energy x-ray diffraction patterns with the beam parallel to the (a) [0, 0, 1] direction, (b) [1, 1, 0] direction, and (c) [1, 1, 1] direction. The left half of each panel is measured at $T = 6$ K well below T_S and the right half at $T = 195$ K above T_S. Superlattice diffraction spots are visible for positions described by a propagation vector (½, ½, 0) but not in the (*H*, *K*, 0) plane in panel (a).

Figure 3. (a) Temperature dependence of the (10, ½, ½) superlattice diffraction peak taken on warming (red symbols) and cooling (blue symbols). The inset shows the temperature region close to the structural order-disorder transition at $T_S = 178$ K and shows the hysteresis in the transition. (b) The temperature dependence of the normalized resistivity of the XRMS sample. A kink corresponding to the structural order-disorder transition is found at T_S.

Figure 4. (a) Specific heat and (b) magnetic susceptibility measurements on the Cd_6Tb sample used for the diffraction measurements. (c) Temperature dependence of the magnetic Bragg peaks from the monoclinic domains close to the bcc (7, 0, 0) position.

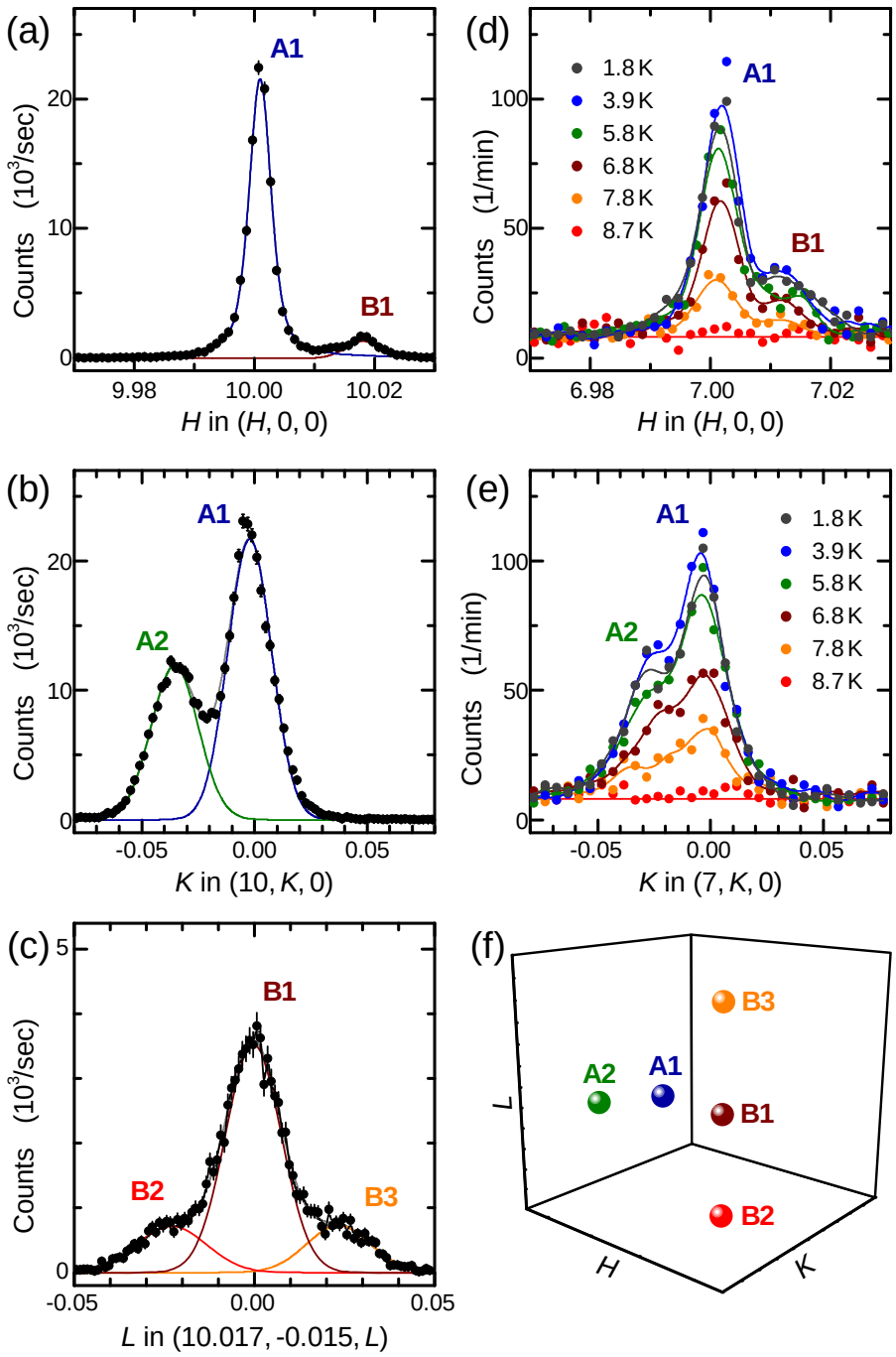
(a)
A1
B1
Counts (10³/sec)
H in (H, 0, 0)
(b)
A1
A2
Counts (10³/sec)
K in (10, K, 0)
(c)
B1
B2
B3
Counts (10³/sec)
L in (10.017, -0.015, L)
(d)
1.8 K
3.9 K
5.8 K
6.8 K
7.8 K
8.7 K
A1
B1
Counts (1/min)
H in (H, 0, 0)
(e)
A1
A2
1.8 K
3.9 K
5.8 K
6.8 K
7.8 K
8.7 K
Counts (1/min)
K in (7, K, 0)
(f)
B3
A2
A1
B1
B2
L
H
K

Figure 1

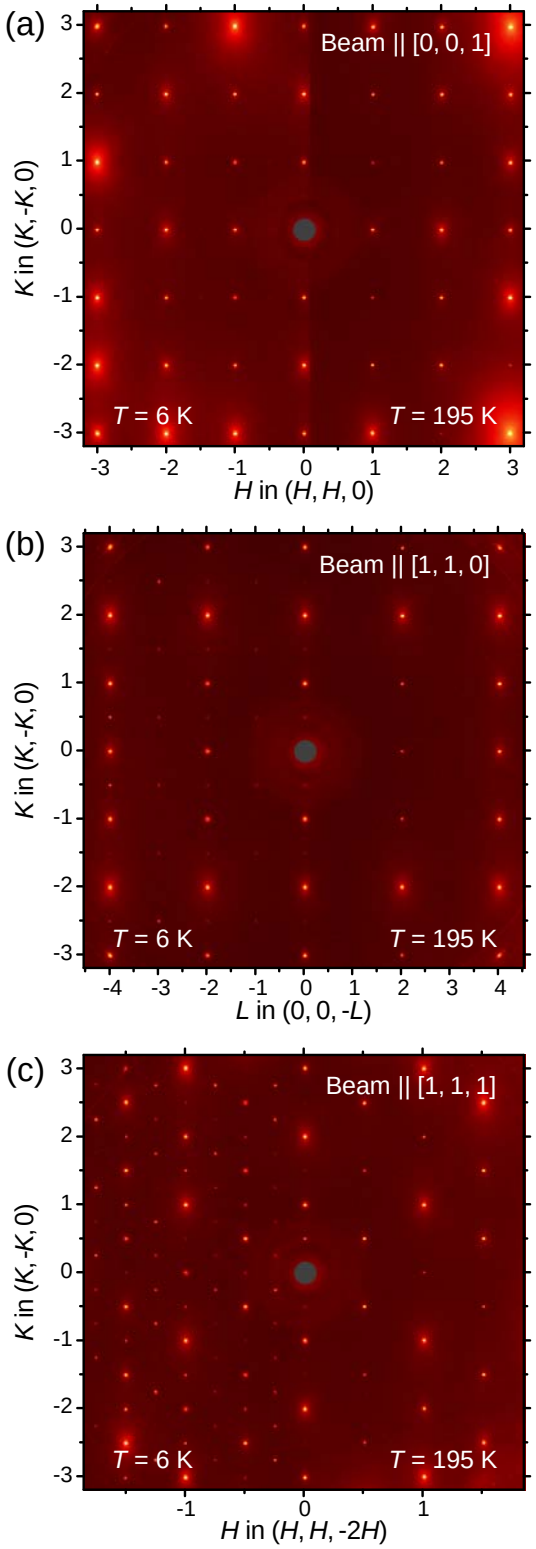
(a)
Beam || [0, 0, 1]
T = 6 K
T = 195 K
K in (K, -K, 0)
H in (H, H, 0)
(b)
Beam || [1, 1, 0]
T = 6 K
T = 195 K
K in (K, -K, 0)
L in (0, 0, -L)
(c)
Beam || [1, 1, 1]
T = 6 K
T = 195 K
K in (K, -K, 0)
H in (H, H, -2H)

Figure 2

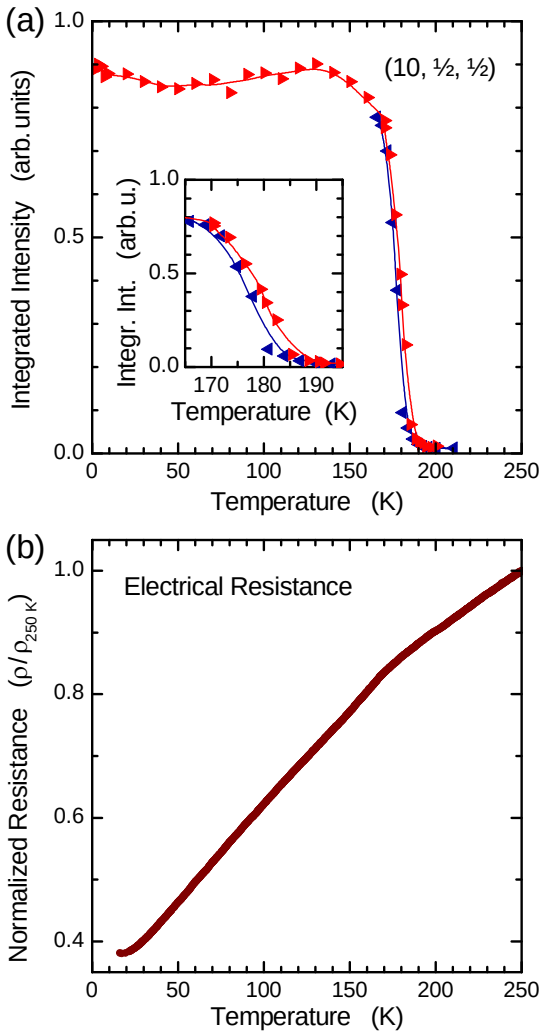
(a)
(10, ½, ½)
Integrated Intensity (arb. units)
Temperature (K)
Integr. Int. (arb. u.)
Temperature (K)
(b)
Electrical Resistance
Normalized Resistance (ρ/ρ250 K)
Temperature (K)

Figure 3

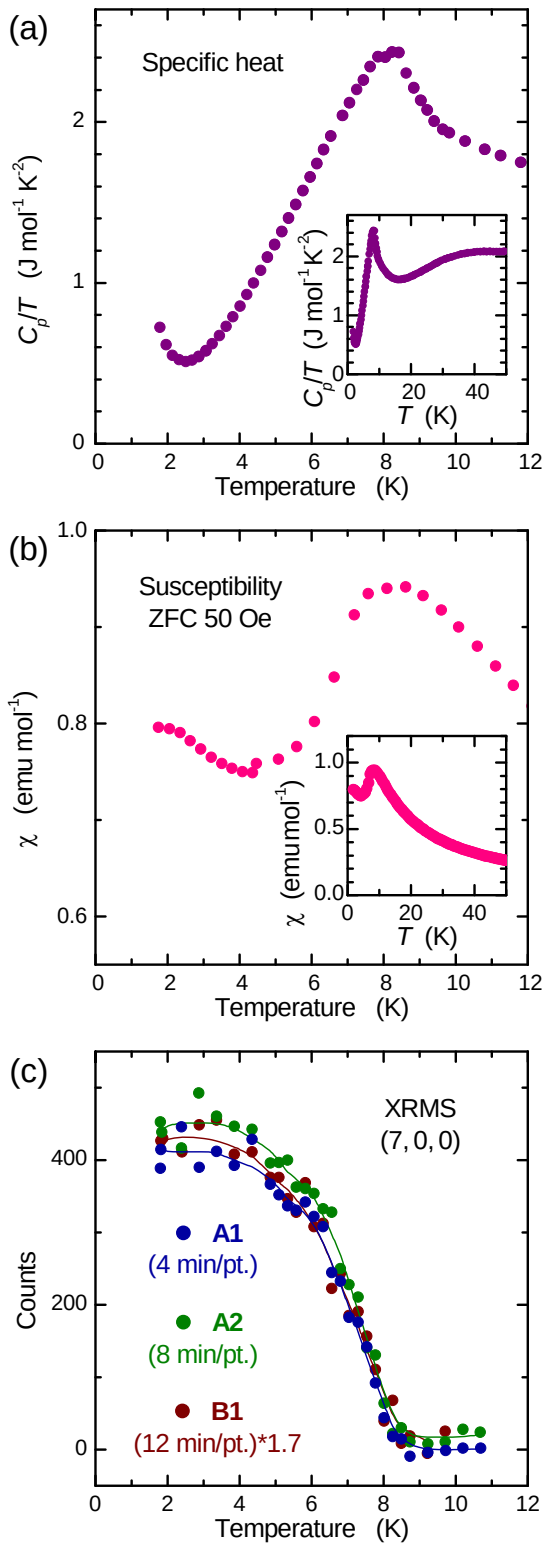
(a)
Specific heat
C_p/T (J mol^{-1} K^{-2})
Temperature (K)
T (K)
(b)
Susceptibility
ZFC 50 Oe
χ (emu mol^{-1})
Temperature (K)
T (K)
(c)
XRMS
(7, 0, 0)
Counts
A1
(4 min/pt.)
A2
(8 min/pt.)
B1
(12 min/pt.)*1.7
Temperature (K)

Figure 4